Applied Catalysis B: Environmental 152–153 (2014) 11–18

Contents lists available at ScienceDirect

Applied Catalysis B: Environmental

journal homepage: www.elsevier.com/locate/apcatb

Ordered mesoporous Cu–Ce–O catalysts for CO preferential oxidation in H_2-rich gases: Influence of copper content and pretreatment conditions

Dong Gu [a], Chun-Jiang Jia [a,b,*], Hans Bongard [a], Bernd Spliethoff [a], Claudia Weidenthaler [a], Wolfgang Schmidt [a], Ferdi Schüth [a,*]

[a] Max-Planck-Institut für Kohlenforschung, Kaiser-Wilhelm-Platz 1, 45470 Mülheim an der Ruhr, Germany
[b] Key Lab for Colloid and Interface Chemistry, School of Chemistry and Chemical Engineering, Shandong University, Jinan 250100, PR China

ARTICLE INFO

Article history:
Received 7 August 2013
Received in revised form 8 January 2014
Accepted 9 January 2014
Available online 19 January 2014

Keywords:
Mesoporous materials
Cu–Ce–O catalysts
Hard-template
CO oxidation

ABSTRACT

Highly ordered mesoporous Cu–Ce–O catalysts with different Cu contents have been synthesized by using ordered mesoporous silica KIT-6 as a hard template. The mesostructural order of the negative replica is influenced by the ratio of Cu to Ce. Using XRD, HR-SEM, TEM and EDX analysis, it was found that the ordered mesostructures of the nanocomposites degenerate with increasing Cu concentration, due to CuO leaching during the template removal process and a phase separation at high Cu concentration. Cu ions can replace Ce-ion in the structure of CeO_2 at Cu concentrations below 40 mol%. However, the Cu concentration in the final materials is lower than expected from the ratio used in the synthesis. The activity in preferential oxidation of CO in H_2-rich gases (PROX) was tested at a space velocity of 60,000 mL h^{-1} g_{cat}^{-1}. The activity of the mesoporous catalysts increases with the concentration of Cu and becomes stable for Cu concentrations higher than 20 mol%. A CO conversion around 100 % can be attained with $Cu_{0.20}Ce_{0.80}O_2$ as catalyst at 160 °C. The exit CO concentration can be as low as 70 ppm under these conditions. The CO_2 selectivity can reach 100 % at low temperature (60 – 80 °C). Direct loading of CuO on the surface of mesoporous CeO_2 leads to large CuO crystals and correspondingly low activity. The influence of the pretreatment atmosphere on activity was also studied. Oxidation–reduction–reoxidation cycling can improve the catalytic activity of the catalysts.

1. Introduction

Among the different kinds of fuel cells, the polymer-electrolyte-membrane fuel cell (PEMFC) is interesting for application in electric vehicles or for residential power-generation because of its many attractive features such as high power density, rapid start-up, and high efficiency [1]. If the H_2 for PEMFC is produced locally or on board of vehicles, catalytic reforming of hydrocarbons, followed by the water–gas shift (WGS) reaction is usually the method of choice [2,3]. The WGS reaction is exothermic and thermodynamically limited. Consequently, high CO conversion is only achieved at low temperature. Unfortunately, conventional WGS catalysts have relatively low activities at low temperatures. Therefore, approximately 1 vol% of CO usually remains in the hydrogen stream after the shift stage. Since the platinum based anode catalyst of the fuel cell is poisoned by CO, CO should be removed to a trace level, namely to below 10 ppm for pure Pt anode catalysts, and to below 100 ppm for CO-tolerant alloy anodes [1,4]. Preferential oxidation of CO (PROX), after addition of small amounts of oxygen to the hydrogen-rich stream, is considered as one of the most straightforward and cost-effective methods to achieve acceptable CO concentrations. For PROX, supported noble metal alloy catalysts, based on Ru and Pt, are currently the benchmark systems [5–9].

As a noble metal-free alternative, the Cu–Ce–O system is a promising candidate, due to its low cost and high selectivity [1,7,10–12]. The influence of preparation method, promoters, and even pretreatment conditions on the catalyst performance have been studied [1,13–22]. Although many of the catalysts described have good activities, the temperature window for high CO-conversion and acceptable selectivity are often quite narrow under realistic conditions. Exit CO concentrations down to the ppm level have rarely been reported over the Cu–Ce–O catalyst system. The catalytic properties depend strongly on the preparation method and the interface between CuO and CeO_2 species [23,24]. The reduction of the particle size of the catalyst to the nanoscale

* Corresponding authors at: Max-Plank-Institut für Kohlenforschung, Department of Heterogeneous Catalysis, Kaiser-Wilhelm-Platz 1, Mülheim an der Ruhr 45470, Germany. Tel.: +49 208 3062373; fax: +49 208 3062995.
E-mail addresses: jiacj@sdu.edu.cn (C.-J. Jia), schueth@mpi-muelheim.mpg.de (F. Schüth).

0926-3373/$ – see front matter © 2014 Elsevier B.V. All rights reserved.
http://dx.doi.org/10.1016/j.apcatb.2014.01.011

leads to increased specific surface area and creates more surface defects, leading to higher activity.

One of the effective methods to prepare nanosized catalysts is nanocasting. Using mesoporous silica as a sacrificial template to prepare metal oxides with high surface areas and small crystallite sizes is one of the most versatile methods. The nanocasting method has obvious advantages in the synthesis of catalysts [25]. (a) Uniform and small crystallite size, usually smaller than 10 nm; (b) high surface area and uniform pore size; (c) adjustable structure; and (d) crystalline framework, with domain sizes that do not increase with increase in synthesis temperature. Because of the weakly amphoteric properties of CuO, which results in reaction with the concentrated alkali solution used during silica template removal, the hard-templating synthesis of ordered mesoporous CuO using mesoporous silica has seldom been reported [26]. Addition of ceria as additional compound could lead to formation of ternary oxides, and stabilize the mesostructure. Ordered mesoporous metal oxide composites containing CuO species are thus accessible. Several groups have used the nanocasting technique to synthesize Cu–Ce–O catalysts for WGS [27,28] and PROX [23] reactions. Such types of catalyst with high surface area and highly crystalline framework show unexpectedly high catalytic reactivity in CO-PROX. However, systematic studies on the dependence of catalytic performance on the amount of copper incorporated, the leaching of CuO, and the influence of the leaching on the catalytic activity, have not been studied, yet.

Herein, we report the preparation of ordered mesoporous Cu–Ce–O catalysts by the nanocasting method, and their catalytic performance in CO-PROX. The amount of Cu incorporated was varied by changing the concentration of the Cu precursor from 5 to 70 mol%. As much as 40 mol% of Cu can be incorporated in the framework of CeO_2 without obvious formation of a separate copper compound, and 30.3 mol% are left after leaching to remove the template. The catalytic performance of those catalysts changes in a regular manner with the incorporated Cu amount. The best catalytic performance was observed for the sample $Cu_{0.20}Ce_{0.80}O_2$. The CO concentration could be reduced to levels as low as 70 ppm over this catalyst. Oxidation–reduction–reoxidation pretreatment was found to improve the performance of the catalysts.

2. Experimental

2.1. Catalyst synthesis

Mesoporous silica KIT-6 hard template was prepared under hydrothermal conditions at 110 °C for 24 h, according to established procedures [29]. Highly ordered mesoporous Cu–Ce–O composite catalysts were prepared by the nanocasting method with mesoporous silica KIT-6 as a hard template. The $Cu(NO_3)_2{\cdot}3H_2O$ and $Ce(NO_3)_3{\cdot}6H_2O$ precursors with different Cu/Ce ratios (from 5:95 to 70:30) were incorporated in the channels of mesoporous silica *via* an evaporation assisted impregnation process [30,31]. The subsequent decomposition of the precursors was carried out in a muffle oven at 600 °C. Finally, the mesoporous silica hard template was leached by hot NaOH solution (2 M, 100 mL, 70 °C). The catalysts nanocast from KIT-6 were labeled as $Cu_xCe_{1-x}O_2$ ($x = 0.05$–0.70). For a typical procedure, 0.24 g of $Cu(NO_3)_2{\cdot}3H_2O$ (1.0 mmol) and 1.74 g of $Ce(NO_3)_3{\cdot}6H_2O$ (4.0 mmol) were dissolved in 20 mL of ethanol. Then 0.74 g of KIT-6 (pore volume: 1.34 $cm^3\,g^{-1}$) was added under continuous stirring. After stirring for 2 h, the solvent was evaporated at room temperature. The residual powder was dried at 60 °C over night and then transferred into a muffle oven and annealed (heating rate 1 °C min^{-1}) at 600 °C for 5 h in air. Finally, the mesoporous silica hard template was etched by hot NaOH solution (2 M, 100 mL, 70 °C). Before use in catalytic experiments, the Cu–Ce–O catalyst powder was pressed, crushed, and sieved to 20 - 40 mesh. For comparison, a two-step method was used to prepare a CuO (20 mol%) loaded mesoporous CeO_2 catalyst. Briefly, 4.0 mmol $Ce(NO_3)_3{\cdot}6H_2O$ was first incorporated into the pore system of KIT-6, then the cerium precursor was transformed into CeO_2 inside the template by calcination of the composite at 350 °C for 6 h in air. Then 1.0 mmol of $Cu(NO_3)_2{\cdot}3H_2O$ was incorporated into the former composite material, and calcined at 600 °C for 5 h in air. Finally, the silica template was removed in hot NaOH solution (2 M, 100 mL, 70 °C). The obtained catalyst was denoted as CuO (20%) on CeO_2.

2.2. Characterization

Powder X-ray diffraction (XRD) patterns were recorded on a Stoe θ–θ diffractometer operating in reflection mode with Cu $K\alpha_{1,2}$ radiation that was monochromatized with a secondary graphite monochromator. The nitrogen adsorption–desorption measurements were performed on a NOVA 4200e instrument at 77 K. Prior to the measurements, all samples were degassed under vacuum for at least 6 h at 150 °C. The BET surface area was calculated from the data in a relative pressure range from 0.05 to 0.20. By using the Barrett–Joyner–Halenda (BJH) algorithm, the pore volumes and pore size distributions were derived from the adsorption branches of isotherms (normally desorption is recommended, but the desorption branches could be influenced by the tensile strength effect). High-resolution scanning electron microscope (HR-SEM) images, and scanning transmission electron microscope (STEM) images, were taken on a Hitachi S-5500 ultrahigh-resolution cold field emission scanning microscope with a Thermo Scientific NORAN System 7 X-ray Microanalysis unit at an acceleration voltage of 30 kV. Morphological and structural characterization of the catalysts was performed with a Hitachi H-7100 at an acceleration voltage of 100 kV or with a Hitachi HF2000 microscope equipped with a cold field emission gun and a Noran energy dispersive X-ray (EDX) unit at an acceleration voltage of 200 kV. The EDX results were calculated from the results of several selected areas on Hitachi HF2000 or conducted on a Hitachi S-3500N scanning electron microscope. Temperature-programmed reduction (TPR) experiments were performed with an in-house constructed system, equipped with a thermal conductivity detector (TCD) to measure H_2 consumption. 50 mg sample was reduced with a 4.5 vol% H_2/N_2 mixture (30 mL min^{-1}) by heating up to 450 °C at a rate of 10 °C min^{-1}.

2.3. Catalytic testing

The catalytic activity for CO-PROX in H_2-rich gases was measured in a plug flow reactor by use of defined amount of catalyst (50 mg of catalyst with a grain size of 250 – 500 μm was mixed with 200 mg quartz sand, SV = 60,000 mL h^{-1} $g_{cat}{}^{-1}$) in a gas mixture of 1.0 vol% CO, 1.0 vol% O_2, 50 vol% H_2 and N_2 balance. Temperatures during the catalytic tests are always referred to the value measured with a thermocouple placed in the catalyst bed, while a thermocouple for oven control was placed outside of the reactor tube. Before measurement, the catalysts were first activated *in situ* in synthetic air (20 vol% O_2/80 vol% N_2 mixture, from Air Liquide, 99.997% purity) at 300 °C for 60 min, cooled in nitrogen flow to 40 °C, then activity curves were recorded as described below. A second activity *vs.* temperature curve was recorded after treatment of the catalyst in a gas mixture consisting of 20 vol% H_2 in N_2 at 300 °C for 30 min with a flow rate of 50 mL min^{-1} and cooling in nitrogen to 40 °C. A third curve was then taken after again pre-treating the catalyst in synthetic air as described above (oxidation–reduction–reoxidation). For a typical temperature *vs.* activity curve, the temperature was increased in 20 °C steps from

40 °C (5 min ramp time between the plateaus) to the final temperature (260 °C). The concentrations of CO and CO_2 were analyzed with nondispersive infrared (IR) spectroscopy, and O_2 was analyzed with a paramagnetic analyzer at the outlet of the reactor on three URAS 3E analyzers (ABB, EL3020, Hartmann and Braun). Before the data point was taken, the catalyst was equilibrated under reaction conditions for 30 min, after this time typically a stationary state was reached. Then the temperature was increased stepwise to assess the performance of the catalysts at different temperatures. The values for conversion of CO (X_{CO}) and selectivity to CO_2 (S_{CO_2}) in the CO-PROX process are defined as following:

$$X_{CO} = \frac{F_{CO}^{in} - F_{CO}^{out}}{F_{CO}^{in}} \times 100\%, \quad X_{O_2} = \frac{F_{O_2}^{in} - F_{O_2}^{out}}{F_{O_2}^{in}} \times 100\%,$$

$$S_{CO_2} = \frac{X_{CO} F_{CO}^{in}}{2X_{O_2} F_{O_2}^{in}} \times 100\%$$

where X and S are percentage conversion and selectivity, respectively, and F is the (inlet or outlet) molar flow of the indicated gas.

3. Results and discussion

3.1. Catalyst characterization

Mesoporous silica KIT-6 with space group of $Ia\bar{3}d$ was synthesized according to literature [29] and used as a hard template. The pore volume and specific surface area of mesoporous silica templates vary by changing the aging temperature; here an aging temperature of 110 °C was used for the synthesis of the KIT-6 silica template. The obtained KIT-6 silica template with highly ordered mesostructure has a large pore volume (1.34 $cm^3\,g^{-1}$) and high specific surface area (882 $m^2\,g^{-1}$) (Table 1 and Supporting information Figs. S1 and S2). Highly ordered mesoporous Cu–Ce–O composite materials with different Cu/Ce ratios were synthesized using the KIT-6 as hard template. The Cu/Ce ratio can be adjusted by changing the molar ratio of the precursors. The small-angle XRD patterns (Fig. 1A) of the replica Cu–Ce–O catalysts all have well resolved diffraction peaks, indicating ordered mesostructured materials. For instance, the pattern of $Cu_{0.20}Ce_{0.80}O_2$ shows five reflections (Fig. 1Ad) which can be indexed as (2 1 1), (2 2 0), (3 1 1), (3 3 0/4 1 1), and (4 2 2) reflections of the $Ia\bar{3}d$ space group, characteristic for the bicontinuous cubic structure. The diffraction pattern indicates a highly ordered mesostructured material. The cell parameter (a_0) of $Cu_{0.20}Ce_{0.80}O_2$ is calculated to be 22.8 nm (Table 1), close to the 23.5 nm of the mother template KIT-6. This indicates good replication of the silica template, the mesostructure is retained very well after template removal, although the template was only impregnated once with the precursor solutions. The mesoscale cell parameters of all Cu–Ce–O catalysts with different Cu/Ce ratios are similar, due to the good replication of the silica template, which confirms that the obtained Cu–Ce–O catalysts are true replicas of the KIT-6 pore structure.

Wide-angle XRD (WAXRD) patterns (Fig. 1B) of the Cu–Ce–O catalysts show well resolved broader reflections that can be assigned to the *fcc* fluorite CeO_2 phase (PDF data file 00-043-1002), indicating well-crystallized nanomaterials. With increasing Cu/Ce ratio, the diffraction peaks shift to higher angles which may be related to the substitution of copper into cerium sites (Fig. S3). No peaks belonging to any ordered copper phase were detected for samples with Cu/Ce below 40/60. This indicates that the copper species are homogeneously dispersed in the CeO_2 matrix either in the form of solid-solution compounds or in the form of particles with such a small domain size that they could not be detected by XRD [28,32]. The domain sizes calculated from XRD data with the Scherrer formula are 5 – 6 ± 1 nm, which is a little smaller than the average pore size of the KIT-6 template (9.2 nm), indicating the confined growth of the oxide crystals inside the pore channels of the template. Interestingly, when the Cu/Ce ratio increases to 50/50, two narrow diffraction peaks at around 35.5 and 38.7° (2θ) are observed (Fig. 1Bg). These peaks can be attributed to the (0 0 2) and (1 1 1) reflections of monoclinic CuO with the space group *C*2/*c* (PDF data file 00-045-0937). This suggests that at higher copper amounts an additional separate copper phase forms. When the Cu/Ce ratio increases to 70/30, more reflections belonging to CuO are observed (Fig. 1Bh). For the sample impregnated in two steps, the CuO reflections can also be observed in the WAXRD pattern (Fig. 1B) even though the CuO loading is only 20 mol%, suggesting the formation of a separate CuO phase.

HR-SEM images (Fig. 2) of the replica Cu–Ce–O catalysts show aggregated spherical particles with particle sizes in the range from tens of nanometers to several hundred nanometers. These spherical particles are composed of sub-10 nm nanoparticles which form an interpenetrating network structure, as observed in our previous work [33,34]. No bulk crystalline particles were observed, indicating that almost all of the precursors had successfully been incorporated into the silica pore system, and no copper–cerium-oxide particles had grown outside of the pore system in the following calcination step. The retention of the replica bicontinuous mesostructure indicates that the silica template aged at 110 °C contains a high fraction of large micropores or small mesopores within the walls which connect the two separate mesopore systems. The size of the individual crystallites forming the Cu–Ce–O composite particles was estimated to be ~8 nm (Fig. 2d inset), corresponding very well with the XRD results, further confirming the growth of the nanocrystals inside the channels. The smaller particle sizes compared to the pore size of the template may occur due to the high volume shrinkage (to 24.0 % for $Ce(NO_3)_3{\cdot}6H_2O$ and to 12.1 % for $Cu(NO_3)_2{\cdot}3H_2O$) and low loading amount [35]. So only a fraction of the template pore volume was filled with Cu–Ce–O composite oxides after decomposition of the precursors by calcination.

TEM images of the replica Cu–Ce–O composite catalysts with different Cu/Ce ratios (Cu below 20 %) are shown in Fig. 3 and Fig. S4. All samples have well-ordered frameworks despite the small particle dimensions. Even if some of the replica Cu–Ce–O composite particles are quite small, the TEM images give a clear indication that the crystalline domain size is in agreement with the pore size of the silica template, further confirming that the Cu–Ce–O phase was formed predominantly inside the porous silica phase. If the Cu/Ce ratio increases to above 30/70, less ordered materials are obtained (Fig. 3). Some irregularly shaped particles with honeycomb pores can be found in sample $Cu_{0.50}Ce_{0.50}O_2$ (Fig. 3h), which may form due to the CuO leaching from the composite crystals. Combined with the WAXRD results, one may assume that at such high concentrations the copper species cannot fully be dissolved within the CeO_2 matrix; and they are also not fully incorporated in a possible, surface segregated amorphous phase. As a result, formation of the pure CuO phase occurs. On the other hand, for the CuO loaded CeO_2 sample, big crystalline particles can be observed (Fig. 3j–l). Selected area EDX results (not shown here) prove that the big crystals consist of pure CuO. This suggests that for the two-step filling method the CuO phase grows outside the silica pore system which could be due to the volatilization of copper nitrate at 227 °C.

The copper contents for the sample series, as calculated from the EDX results, are summarized in Table 1. The Cu content for $Cu_{0.05}Ce_{0.95}O_2$ is only 4.0 mol%, indicating that about 20 % of the copper species is either not incorporated or lost during the template removal process due to the slightly amphoteric properties of CuO. A similar trend is observed for all the other samples: the copper content in the final material is about 20 – 30% lower than would correspond to the copper offered in the synthesis. After dissolution

Table 1
Physicochemical properties and PROX activities of mesoporous Cu–Ce–O catalysts with different compositions.

Sample name	Cell parameter a_0 (nm)[a]	BET surface area ($m^2\ g^{-1}$)	Pore volume ($cm^3\ g^{-1}$)	$T_{Con\text{-}Sel}$ (°C)[b]	Conversion (%)[c]	Cu content (%)[d]
KIT-6	23.5	882	1.34	–	–	–
$Cu_{0.05}Ce_{0.95}O_2$	23.5	135	0.55	197(200)	59(57)	4.0
$Cu_{0.10}Ce_{0.90}O_2$	23.5	133	0.52	155(161)	78(75)	9.1
$Cu_{0.15}Ce_{0.85}O_2$	24.5	138	0.51	131(146)	87(84)	12.1
$Cu_{0.20}Ce_{0.80}O_2$	22.8	122	0.32	124 (134)	90 (86)	14.0
$Cu_{0.30}Ce_{0.70}O_2$	22.0	155	0.56	128	88	21.7
$Cu_{0.40}Ce_{0.60}O_2$	22.5	159	0.52	127	87	30.3
$Cu_{0.50}Ce_{0.50}O_2$	23.0	105	0.22	127	88	45.3
$Cu_{0.70}Ce_{0.30}O_2$	22.5	73	0.12	129	88	69.1
CuO (20%) on CeO_2	23.5	108	0.40	138	86	19.1

[a] Calculated from the small-angle XRD results by formula $a_0 = \sqrt{6} \times d_{211}$.
[b] Temperatures of the cross-over points of conversion equal to selectivity, the numbers in brackets are repeat results with new samples.
[c] CO conversions at the cross-over points of conversion equal to selectivity, the numbers in brackets are repeat results with new samples.
[d] Cu contents calculated from TEM-EDX results for copper content below 40%. Other samples calculated from SEM-EDX results.

of the silica template, the NaOH solution was blue, indicating a substantial concentration of Cu^{2+} in the alkaline solution. This means that the NaOH solution at least partly dissolves CuO under the silica removal conditions.

The nitrogen adsorption–desorption isotherms (Fig. 4) of the Cu–Ce–O replicas are similar. They are characterized by a small capillary condensation step at relative pressures around 0.3 – 0.5 that is attributed to the mesopores produced by the removal of the silica walls, and another broad capillary condensation step at high relative pressure (P/P_0 = 0.8 – 0.9), related to the textural pores between the particles. The corresponding BET surface areas and total pore volumes of all samples are summarized in Table 1. The BET surface areas for all the single-phase samples are between 120 and 160 $m^2\ g^{-1}$. This is quite high, considering the high density of the metal oxides and the low level of microporosity. For samples with a Cu content exceeding 50 % or the sample with CuO loaded onto CeO_2, the BET surface area is substantially smaller, due to the formation of big CuO crystals.

Results obtained by H_2-TPR experiments are presented in Fig. 5 and Table S1. Two typical peaks can be observed for the Cu–Ce–O composite catalysts with Cu contents below 40 % (Fig. 5b–g). The broad one at low temperature (around 200 °C, called α peak) can be attributed to the reduction of well-dispersed surface copper species, while the sharper one at higher temperature can be assigned to the reduction of copper in the CeO_2 framework (called β peaks) [23,36]. The α peak positions of the samples with different copper contents show no big difference, suggesting that the surface copper species are quite similar for all the samples after treatment with NaOH aqueous solution during the silica removal process. The H_2 consumption corresponding to the α peak is rather similar for all samples with copper content below 40 mol% which further confirms the suggested similarity of the surface copper species (Table S1). The β peak positions exhibit a regular variation: the temperature decreases from 340 to 233 °C with the increase in copper content (340 °C (5 %), 282 °C (10 %), 256 °C (15 %), 240 °C (20 %), 227 °C (30 %), and 233 °C (40 % Cu)), in addition, the peak areas increase with copper content. These observations suggest that the increase in the concentration of framework copper species promotes the formation of defects, thus decreasing the reduction temperature of framework copper. In addition, the higher copper concentration could facilitate the nucleation of metallic copper, which also would tend to lower the reduction temperature. For the samples with separate CuO phase, a third peak appears at higher temperature (Fig. 5h–i), which can be attributed to the reduction of CuO particles. The temperature of the β peak of Cu (20 %) loaded sample at 235 °C is very close to the one for $Cu_{0.20}Ce_{0.80}O_2$,

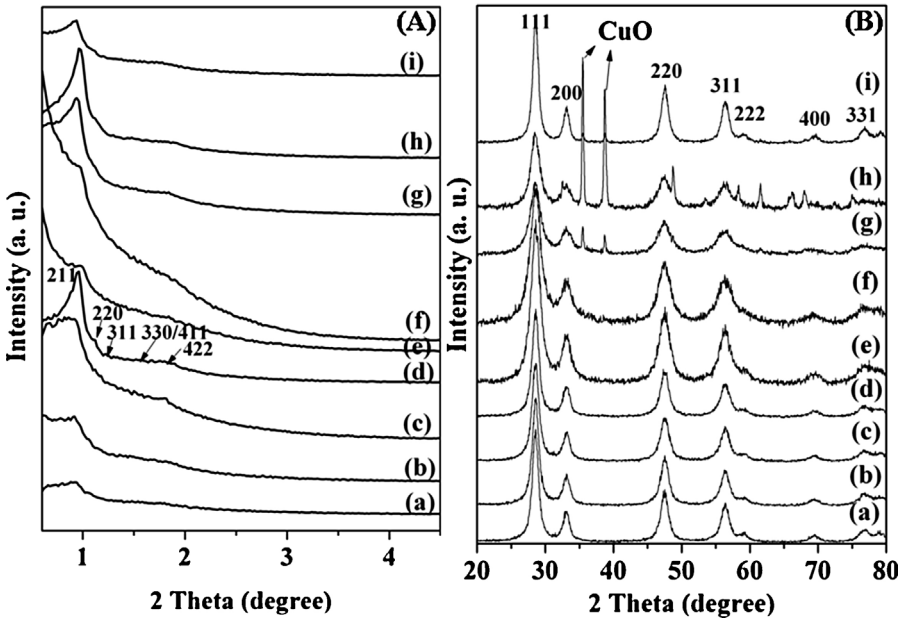

Fig. 1. XRD (A) and WAXRD (B) patterns of mesoporous (a) $Cu_{0.05}Ce_{0.95}O_2$, (b) $Cu_{0.10}Ce_{0.90}O_2$, (c) $Cu_{0.15}Ce_{0.85}O_2$, (d) $Cu_{0.20}Ce_{0.80}O_2$, (e) $Cu_{0.30}Ce_{0.70}O_2$, (f) $Cu_{0.40}Ce_{0.60}O_2$, (g) $Cu_{0.50}Ce_{0.50}O_2$, (h) $Cu_{0.70}Ce_{0.30}O_2$, and (i) CuO (20%) on CeO_2.

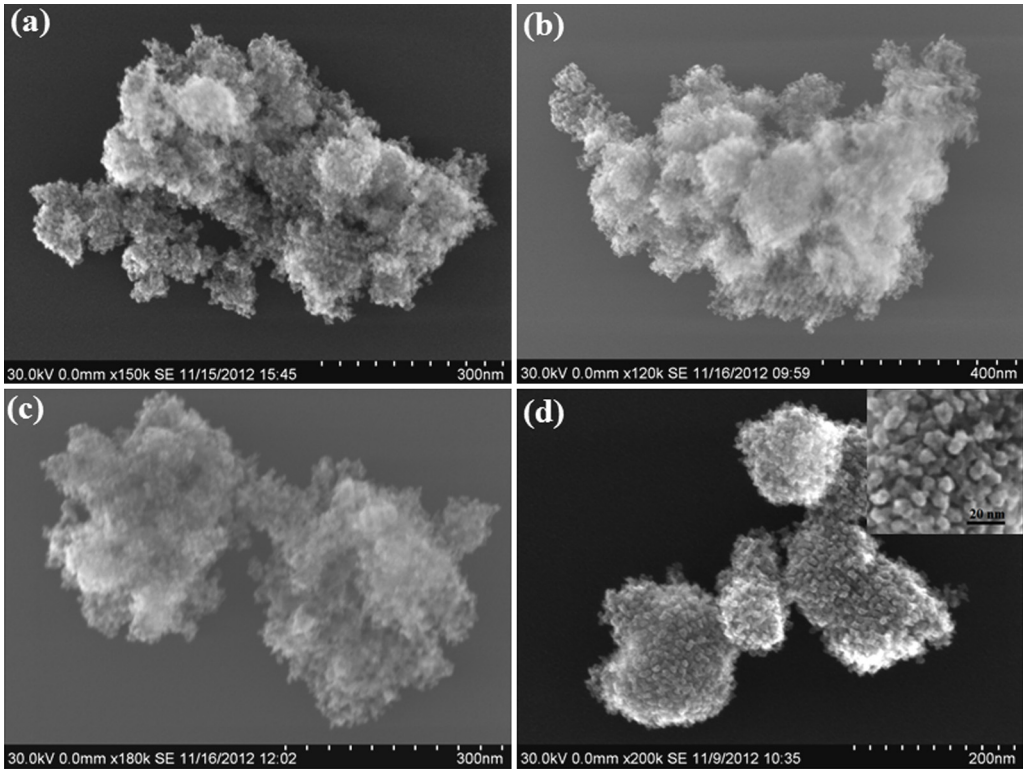

Fig. 2. HR-SEM images of mesoporous materials: (a) $Cu_{0.05}Ce_{0.95}O_2$; (b) $Cu_{0.10}Ce_{0.90}O_2$; (c) $Cu_{0.15}Ce_{0.85}O_2$; and (d) $Cu_{0.20}Ce_{0.80}O_2$.

suggesting that the copper species are partially introduced into the CeO_2 lattice due to the heat treatment at high temperatures (at 600 °C). In addition, the total H_2 consumption for both samples, $Cu_{0.20}Ce_{0.80}O_2$ and Cu20 loaded CeO_2, are almost identical, suggesting a similar copper content. However, the H_2 consumption corresponding to the α peak for the Cu20 loaded sample is roughly only half of that determined for sample $Cu_{0.20}Ce_{0.80}O_2$. The β peak for Cu20 loaded sample is also smaller than for the composite one; instead, a third peak corresponding to the reduction of CuO particles appears. All those results suggest that part of the copper species is introduced into the CeO_2 lattice for the impregnated sample, but the amount is much lower than for the composite. The total H_2 consumption increases from 0.90 to 5.90 mmol g^{-1} with the copper content increasing from 5 to 70 mol% (Table S1). Those amounts are substantially higher than what would be needed for reduction of all copper species, implying the CeO_2 is at least partially reduced at low temperature (below 400 °C). This suggests that the doping of copper into the CeO_2 framework facilitates also the reduction of ceria species by H_2 at low temperature [37].

3.2. CO-PROX activity tests

The catalytic activity and selectivity for CO-PROX of Cu–Ce–O catalysts after an "oxidation–reduction–reoxidation" cycle against temperature are given in Fig. 6 and in addition summarized in Table 1. Each data point was recorded after keeping the catalyst at that temperature under reaction conditions for 30 min, sufficient for reaching a steady state. Sample $Cu_{0.20}Ce_{0.80}O_2$ shows the best results among all the catalysts. 100 % CO conversion can be reached at around 160 °C. The exit CO concentration at this temperature is as low as 70 ppm. However, at this temperature also some H_2 oxidation takes place, and high selectivity is only obtained at lower temperature. 100 % CO_2 selectivity is observed between 80 and 100 °C. A characteristic single point characterizing catalyst performance is the cross-over point of the conversion and selectivity curves (Table 1). The temperature of the cross-over point decreases from 200 to 124 °C with increase in copper content from 5 % to 20 %. At higher copper content a plateau is reached at around 127 °C. Conversion/selectivity at the cross-over point increases from 59 % to 90 % with copper concentration increasing from 5 % to 20 %. As for the temperature, conversion/selectivity also reaches a plateau around 88 % at copper contents above 30 %. The T_{50} (temperature for 50 % CO conversion) results show a similar trend, $Cu_{0.05}$ (186 °C) > $Cu_{0.10}$ (130 °C) > $Cu_{0.15}$ (100 °C) > $Cu_{0.20}$ (92 °C) < $Cu_{0.30}$ (97 °C) = $Cu_{0.40}$ (97 °C) ≈ $Cu_{0.70}$ (98 °C). Several catalysts were re-synthesized and evaluated with respect to catalytic performance in order to check reproducibility (results in brackets). Deviations are typically within a few Kelvin, meaning that the trends described are highly significant. Combined with the WAXRD and TPR results described above, this indicates that the concentration of the lattice copper species, which seems to be most relevant for the catalytic performance, reaches a saturation level between 20 % and 40 %. At copper concentrations exceeding 40 % a separate CuO phase is formed, either in the form of small crystals or as separate bulk crystals. Between 20 % and 40 %, no additional phase is visible in the XRD pattern, but the TPR trace changes slightly; the β peak is broadened for the higher concentrations. This could suggest formation of a different copper species which is X-ray amorphous and does not contribute to improved catalytic performance, since the best performing catalyst is the Cu20 sample, although its performance is not significantly better than that of the samples with higher copper content (the resynthesized catalyst of this composition performs slightly worse than the ones with higher copper loading, Table 1). However, this is not proven, yet, and requires further analysis.

The reference sample, 20 % CuO loaded CeO_2, prepared by a two-step impregnation method, has a lower catalytic activity for CO-PROX than the composite sample. Only 86 % conversion and selectivity is reached at around 138 °C. This suggests that the one step nanocasting method has a clear advantage over the two-step

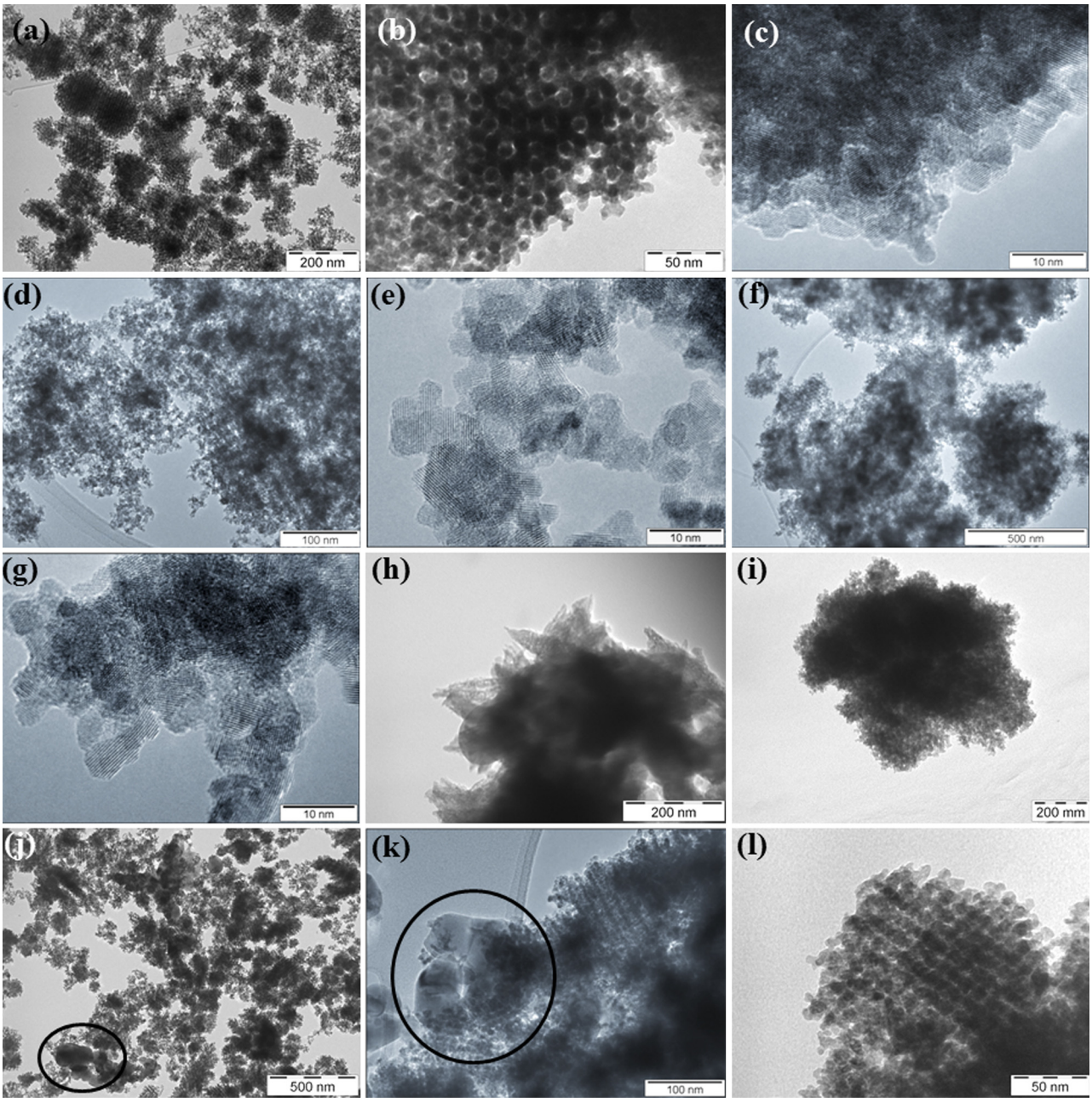

Fig. 3. TEM images of mesoporous materials: (a–c) $Cu_{0.20}Ce_{0.80}O_2$; (d and e) $Cu_{0.30}Ce_{0.70}O_2$; (f and g) $Cu_{0.40}Ce_{0.60}O_2$; (h) $Cu_{0.50}Ce_{0.50}O_2$; (i) $Cu_{0.70}Ce_{0.30}O_2$; and (j–l) CuO (20 %) on CeO_2.

loading method for the preparation of composite catalysts. The one step method allows incorporation of copper in the cerium framework, while for the two-step synthesis separate CeO_2 and CuO phases are generated. Some of the catalysts described in Ref. [23] perform better than the ones studied here. This could be due to either the different concentrations used in the catalytic tests (higher concentration of hydrogen which could leaded to partial copper reduction to Cu^+), to the lower space velocity, or to differences in the nature of the catalyst. The synthesis protocol used in Ref. [23] is somewhat more complicated in that it requires an addition refluxing step in hexane and three silica leaching cycles at room temperature, which leads to higher copper retention in the catalysts. However, our catalysts are better than most traditional $CuO–CeO_2$ catalysts prepared by the co-precipitation or impregnation methods. Kim *et al.*[38] observed ~100 % CO conversion at around 165–175 °C with a 20 % $CuO–CeO_2$ catalyst synthesized by co-preciption. The exit CO concentration is about 10 ppm. However, the space velocity is only 250 mL h^{-1} $g_{cat}{}^{-1}$ and the catalyst is not very stable. Gamarra *et al.* [10] used a modified reverse microemulsion method for the synthesis of a $Ce_{0.80}Cu_{0.20}O_2$ catalyst. This catalyst also showed high conversion (~100 % CO conversion) at low temperature (80–90 °C), but one has to note that the space velocity is also very low level (1000 mL h^{-1} $g_{cat}{}^{-1}$) and the selectivity is only ~60 %. For many other catalysts described in literature [14,15,19,20,39–42], not even 100 % CO conversion can be obtained.

In order to determine the influence of pre-treatment conditions on the catalytic reactivity of Cu–Ce–O catalysts, the samples were pre-treated in different atmospheres before CO-PROX tests. As an example, Fig. 7 shows the CO conversion and CO_2 selectivity as a function of temperature, with different pre-treatment atmospheres as parameter, for the $C_{0.20}Ce_{0.80}O_2$ sample. The sample was activated in different atmosphere before each CO-PROX test. First,

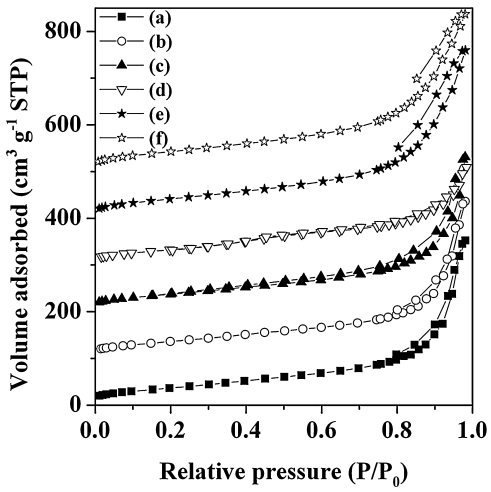

Fig. 4. Nitrogen adsorption–desorption isotherms of (a) $Cu_{0.05}Ce_{0.95}O_2$, (b) $Cu_{0.10}Ce_{0.90}O_2$, (c) $Cu_{0.15}Ce_{0.85}O_2$, (d) $Cu_{0.20}Ce_{0.80}O_2$, (e) $Cu_{0.30}Ce_{0.70}O_2$, and (f) $Cu_{0.40}Ce_{0.60}O_2$. The isotherm of (b), (c), (d), (e) and (f) are offset vertically by 100, 200, 300, 400 and 500 cm^3 g^{-1}, respectively.

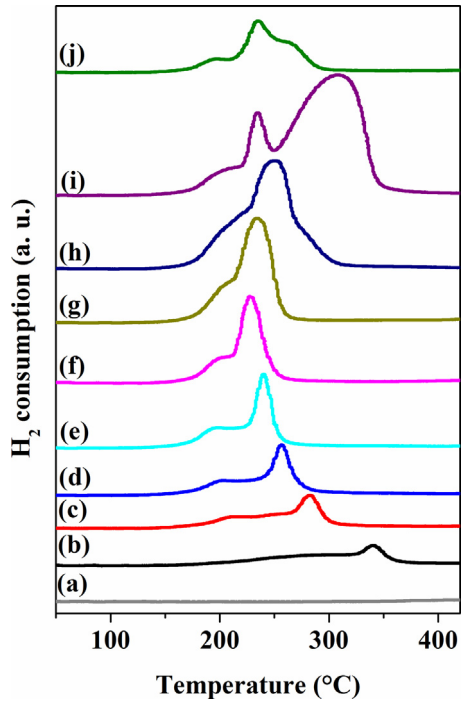

Fig. 5. H_2-TPR profiles of (a) CeO_2, (b) $Cu_{0.05}Ce_{0.95}O_2$, (c) $Cu_{0.10}Ce_{0.90}O_2$, (d) $Cu_{0.15}Ce_{0.85}O_2$, (e) $Cu_{0.20}Ce_{0.80}O_2$, (f) $Cu_{0.30}Ce_{0.70}O_2$, (g) $Cu_{0.40}Ce_{0.60}O_2$, (h) $Cu_{0.50}Ce_{0.50}O_2$, (i) $Cu_{0.70}Ce_{0.30}O_2$, and (j) CuO (20%) on CeO_2 catalysts.

the sample was treated with synthetic air at 300 °C for 60 min, then with 20 vol% H_2 at 300 °C for 30 min, and finally with synthetic air again at this temperature. The corresponding CO-PROX results show a T_{50} of 96, 113 and 92 °C, respectively, suggesting that the oxidation state of copper species plays an important role for the catalytic activity of the catalyst. Cu^+/Cu^{2+} species show higher activity than Cu^0, and the reactivity was improved after the "oxidation–reduction–reoxidation" cycle. The cross-over points of the three groups of curves lie at 90 % (129 °C), 81 % (134 °C), and 90 % (124 °C), respectively, further confirming the improvement in reactivity by redox-cycling. These observations are in line with the results of Martínez-Arias *et al.* [43], who report partially reduced copper (Cu^+) as the most active species.

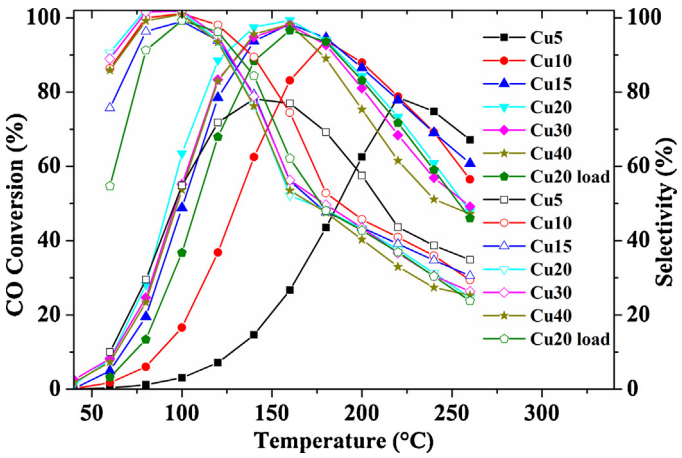

Fig. 6. CO conversion (solid) and CO_2 selectively (open) over Cu–Ce–O catalysts with different Cu/Ce ratios. Operation conditions: WHSV = 60,000 mL h^{-1} g_{cat}^{-1}, 1 vol% CO, 1 vol% O_2, 50 vol% H_2 and N_2 balance.

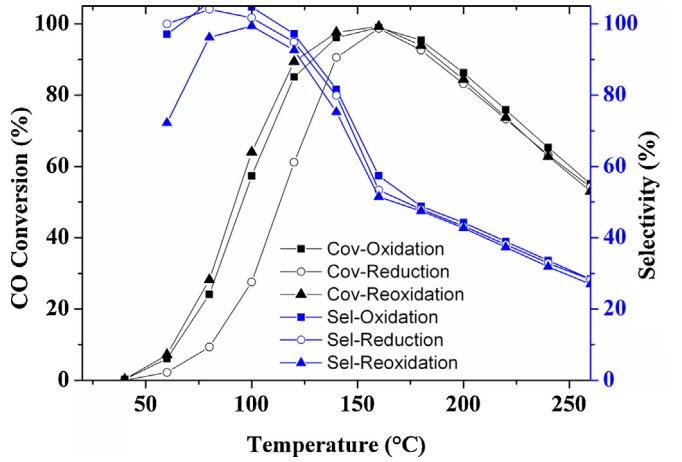

Fig. 7. Influence of pretreatment conditions on the CO conversion and selectivity.

Although there were no obvious changes in the catalyst activity and selectivity after the holding period of 30 min during the catalytic evaluation, slower changes would not be detected in such a test protocol. Therefore, additional catalytic tests under stationary conditions were performed at fixed temperature, also with the aim to check for long term deactivation of the catalysts prepared by the two synthetic protocols. The stability of the $Cu_{0.20}Ce_{0.80}O_2$ and CuO (20 %) on CeO_2 catalysts was tested at 120 °C, since this temperature is close to the cross-over point of conversion and selectivity for the $Cu_{0.20}Ce_{0.80}O_2$ catalyst (Fig. 8). Surprisingly, the CO conversion and CO_2 selectivity over $Cu_{0.20}Ce_{0.80}O_2$ at the beginning of the experiment are as high as 92.6 % and 93.5 %, respectively, which is even somewhat better than the value at the cross-over point. This values decrease slowly to 89.7 % and 90.5 % after keeping the catalyst under reaction conditions at 120 °C for 2 h. The CO conversion stays almost constant afterwards, and the CO_2 selectivity even increases slowly to 100 %. 81 % CO conversion is still retained after a reaction time of 24 h. The 20 % CuO on CeO_2 sample under the same conditions showed an initial CO conversion of only 52.0 %, which slightly decreased to 49.6 % after 2 h, which then remained stable. Both samples had been exposed to the full oxidation–reduction–reoxidation test before the stability test, and during this cycle the 20 % CuO on CeO_2 sample had already suffered some deactivation, since already at the beginning of the test the performance differed more strongly to the $Cu_{0.20}Ce_{0.80}O_2$ sample than in the experiment reported in Fig. 6. These results confirm

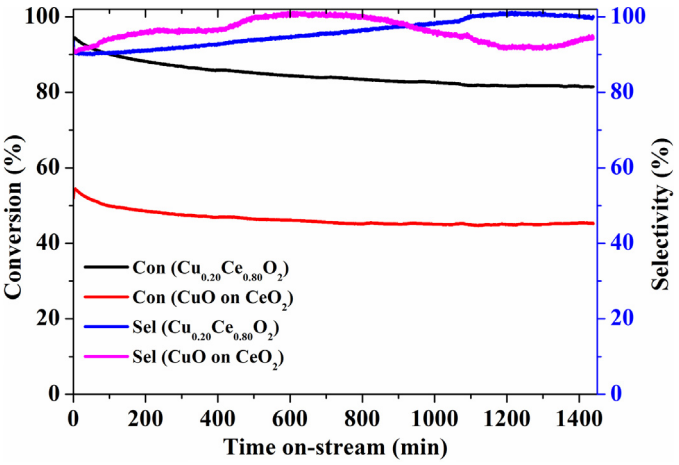

Fig. 8. Performance of the 20 % CuO contains CeO_2 catalysts prepared by different methods at constant temperature of 120 °C. Operation conditions: 50 mg catalyst, 50 mL min^{-1}, WHSV = 60,000 mL h^{-1} g_{cat}^{-1}, 120 °C, 1 vol% CO, 1 vol% O_2, 50 vol% H_2 and N_2 balance.

again that the one step nanocasting method results in material with better catalytic performance compared to the two-step procedure.

4. Conclusion

In summary, ordered mesoporous Cu–Ce–O catalysts with different copper content (5 – 70 mol%) have been successfully synthesized by using mesoporous silica KIT-6 as a hard template in a one-step nanocasting method. The obtained negative replicas show highly ordered $Ia\bar{3}d$ mesostructures with surface areas as high as 159 m^2 g^{-1}. Up to around 40 mol% of copper can be homogeneously dispersed in the framework of the CeO_2 matrix. The catalysts were used in the CO-PROX reaction and show regular activity trends with changing copper amounts. $Cu_{0.20}Ce_{0.80}O_2$ shows the best results, with a CO conversion as high as 100 % at space velocity of 60,000 mL h^{-1} g_{cat}^{-1}. The exit CO concentration can be as low as 70 ppm. The highest CO_2 selectivity reaches 100 % at low temperature (60 – 80 °C). The catalysts nanocast in one step show better performance than the ones prepared by a two-step loading. Furthermore, pre-treatment by an "oxidation–reduction–reoxidation" cycle can improve the reactivity of the catalyst.

Acknowledgment

We greatly acknowledge the support of this research by the Alexander von Humboldt-Stiftung, in addition to the basic support by the Max-Plank-Society.

Appendix A. Supplementary data

Supplementary data associated with this article can be found, in the online version, at http://dx.doi.org/10.1016/j.apcatb.2014.01.011.

References

[1] E.D. Park, D. Lee, H.C. Lee, Catal. Today 139 (2009) 280.
[2] J.R. Rostrup-Nielsen, J. Sehested, J.K. Norskov, Adv. Catal. 47 (2002) 65.
[3] Q. Fu, H. Saltsburg, M. Flytzani-Stephanopoulos, Science 301 (2003) 935.
[4] H.P. Dhar, L.G. Christner, A.K. Kush, J. Electrochem. Soc. 134 (1987) 3021.
[5] E.Y. Ko, E.D. Park, H.C. Lee, D. Lee, S. Kim, Angew. Chem. Int. Ed. 46 (2007) 734.
[6] J. Guzman, S. Carrettin, A. Corma, J. Am. Chem. Soc. 127 (2005) 3286.
[7] G. Avgouropoulos, T. Ioannides, C. Papadopoulou, J. Batista, S. Hocevar, H.K. Matralis, Catal. Today 75 (2002) 157.
[8] R. Farrauto, S. Hwang, L. Shore, W. Ruettinger, J. Lampert, T. Giroux, Y. Liu, O. Ilinich, Ann. Rev. Mater. Res. 33 (2003) 1.
[9] S. Alayoglu, A.U. Nilekar, M. Mavrikakis, B. Eichhorn, Nat. Mater. 7 (2008) 333.
[10] D. Gamarra, G. Munuera, A.B. Hungría, M. Fernández-García, J.C. Conesa, P.A. Midgley, X.Q. Wang, J.C. Hanson, J.A. Rodríguez, A. Martínez-Arias, J. Phys. Chem. C 111 (2007) 11026.
[11] D. Gamarra, C. Belver, M. Fernández-García, A. Martínez-Arias, J. Am. Chem. Soc. 129 (2007) 12064.
[12] A. Gómez-Cortés, Y. Márquez, J. Arenas-Alatorre, G. Díaz, Catal. Today 133 (2008) 743.
[13] G. Avgouropoulos, T. Ioannides, H.K. Matralis, J. Batista, S. Hocevar, Catal. Lett. 73 (2001) 33.
[14] G. Marban, A.B. Fuertes, Appl. Catal., B 57 (2005) 43.
[15] Y. Liu, Q. Fu, M. Flytzani-Stephanopoulos, Catal. Today 93–95 (2004) 241.
[16] C.R. Jung, J. Han, S.W. Nam, T.H. Lim, S.A. Hong, H.I. Lee, Catal. Today 93–95 (2004) 183.
[17] E.Y. Ko, E.D. Park, K.W. Seo, H.C. Lee, D. Lee, S. Kim, Catal. Today 116 (2006) 377.
[18] G. Avgouropoulos, T. Ioannides, Appl. Catal., A 244 (2003) 155.
[19] G. Avgouropoulos, T. Ioannides, H. Matralis, Appl. Catal., B 56 (2005) 87.
[20] G. Avgouropoulos, T. Ioannides, Appl. Catal., B 67 (2006) 1.
[21] R. Kydd, W.Y. Teoh, K. Wong, Y. Wang, J. Scott, Q.H. Zeng, A.B. Yu, J. Zou, R. Amal, Adv. Funct. Mater. 19 (2009) 369.
[22] S. Kandoi, A.A. Gokhale, L.C. Grabow, J.A. Dumesic, M. Mavrikakis, Catal. Lett. 93 (2004) 93.
[23] H. Yen, Y. Seo, S. Kaliaguine, F. Kleitz, Angew. Chem. Int. Ed. 51 (2012) 12032.
[24] A. Hornés, A.B. Hungría, P. Bera, A. López Cámara, M. Fernández-García, A. Martínez-Arias, L. Barrio, M. Estrella, G. Zhou, J.J. Fonseca, J.C. Hanson, J.A. Rodríguez, J. Am. Chem. Soc. 132 (2010) 34.
[25] D. Gu, F. Schüth, Chem. Soc. Rev. 43 (2014) 313.
[26] Y. Ren, Z. Ma, L.P. Qian, S. Dai, H.Y. He, P.G. Bruce, Catal. Lett. 131 (2009) 146.
[27] P. Djinović, J. Batista, A. Pintar, Appl. Catal., A 347 (2008) 23.
[28] P. Djinović, J. Batista, A. Pintar, Catal. Today 147 (2009) S191.
[29] F. Kleitz, S.H. Choi, R. Ryoo, Chem. Commun. (2003) 2136.
[30] A.H. Lu, F. Schüth, Adv. Mater. 18 (2006) 1793.
[31] B.Z. Tian, X.Y. Liu, H.F. Yang, S.H. Xie, C.Z. Yu, B. Tu, D.Y. Zhao, Adv. Mater. 15 (2003) 1370.
[32] W.H. Shen, X.P. Dong, Y.F. Zhu, H.R. Chen, J.L. Shi, Microporous Mesoporous Mater. 85 (2005) 157.
[33] H. Tüysüz, M. Comotti, F. Schüth, Chem. Commun. (2008) 4022.
[34] H. Tüysüz, C.W. Lehmann, H. Bongard, B. Tesche, R. Schmidt, F. Schüth, J. Am. Chem. Soc. 130 (2008) 11510.
[35] X.H. Sun, Y.F. Shi, P. Zhang, C.M. Zheng, X.Y. Zheng, F. Zhang, Y.C. Zhang, N.J. Guan, D.Y. Zhao, G.D. Stucky, J. Am. Chem. Soc. 133 (2011) 14542.
[36] C.G. Maciel, T.d.F. Silva, L.P. Roberto Profeti, E.M. Assaf, J.M. Assaf, Appl. Catal. A 431–432 (2012) 25.
[37] R. Si, J. Raitano, N. Yi, L.H. Zhang, S.W. Chan, M. Flytzani-Stephanopoulos, Catal. Today 180 (2012) 68.
[38] D.H. Kim, J.E. Cha, Catal. Lett. 86 (2003) 107.
[39] F. Marino, C. Descorme, D. Duprez, Appl. Catal., B 58 (2005) 175.
[40] G. Sedmak, S. Hocevar, J. Levec, J. Catal. 213 (2003) 135.
[41] M. Tada, R. Bal, X. Mu, R. Coquet, S. Namba, Y. Iwasawa, Chem. Commun. (2007) 4689.
[42] T. Caputo, L. Lisi, R. Pirone, Ind. Eng. Chem. Res. 46 (2007) 6793.
[43] A. Martínez-Arias, D. Gamarra, M. Fernández-García, A. Hornés, P. Bera, Z. Koppány, Z. Schay, Catal. Today 143 (2009) 211.